Intelligent Automation & Soft Computing

Tech Science Press

DOI: 10.32604/iasc.2023.039836
Article

Predicting Lumbar Spondylolisthesis: A Hybrid Deep Learning Approach

Deepika Saravagi[1], Shweta Agrawal[2,*], Manisha Saravagi[3], Sanjiv K. Jain[4], Bhisham Sharma[5], Abolfazl Mehbodniya[6,*], Subrata Chowdhury[7] and Julian L. Webber[6]

[1]Department of Computer Application, SAGE University, Indore, 452012, Madhya Pradesh, India
[2]IAC, SAGE University, Indore, 452012, Madhya Pradesh, India
[3]Shivang College of Physiotherapy, Ratlam, 4570021, Madhya Pradesh, India
[4]Medi-Caps University, Rau Indore, Madhya Pradesh, 453331, India
[5]Chitkara University Institute of Engineering and Technology, Chitkara University, Punjab, India
[6]Department of Electronics and Communication Engineering, Kuwait College of Science and Technology (KCST), Doha, Kuwait
[7]Department of Computer Science and Engineering, Sreenivasa Institute of Technology and Management Studies, Chittoor, Andra Pradesh, India
*Corresponding Authors: Shweta Agrawal. Email: shweta.cse@sageuniversity.in; Abolfazl Mehbodniya. Email: a.niya@kcst.edu.kw

Received: 20 February 2023; Accepted: 14 April 2023; Published: 23 June 2023

Abstract: Spondylolisthesis is a chronic disease, and a timely diagnosis of it may help in avoiding surgery. Disease identification in x-ray radiographs is very challenging. Strengthening the feature extraction tool in VGG16 has improved the classification rate. But the fully connected layers of VGG16 are not efficient at capturing the positional structure of an object in images. Capsule network (CapsNet) works with capsules (neuron clusters) rather than a single neuron to grasp the properties of the provided image to match the pattern. In this study, an integrated model that is a combination of VGG16 and CapsNet (S-VCNet) is proposed. In the model, VGG16 is used as a feature extractor. After feature extraction, the output is fed to CapsNet for disease identification. A private dataset is used that contains 466 X-ray radiographs, including 186 images displaying a spine with spondylolisthesis and 280 images depicting a normal spine. The suggested model is the first step towards developing a web-based radiological diagnosis tool that can be utilized in outpatient clinics where there are not enough qualified medical professionals. Experimental results demonstrate that the developed model outperformed the other models that are used for lumbar spondylolisthesis diagnosis with 98% accuracy. After the performance check, the model has been successfully deployed on the Gradio web app platform to produce the outcome in less than 20 s.

Keywords: Gradio; lumbar spondylolisthesis; transfer learning; VGG16; machine learning; deep learning

1 Introduction

Spondylolisthesis is the term for the displacement of a vertebrae over the next one [1]. It is a chronic disease that is caused by continuous stress (either by load bearing or bad posture) on the lumbar vertebrae (pars interarticularis). It affects persons of all ages, and a recent study shows that nowadays it is found most commonly in school going children (6%–7%), adults (18%), and elite athletes (7%–8%) [2,3]. According to a study, approximately 50% of low back pain problems in athletes are caused by spondylolisthesis due to hyperextension [4]. 85%–95% of the time, lumbar spondylolisthesis is found between the fifth lumbar vertebrae (L5) and the first sacral vertebrae (S1). The L5-S1 motion segment is the most common region [5,6]. Fig. 1 highlights both regions where lumbar spondylolisthesis may occur.

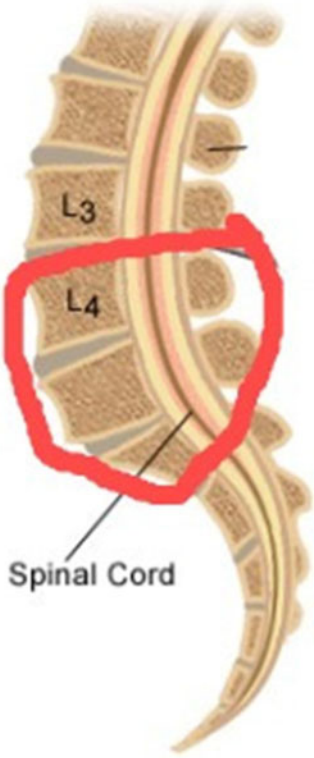

Figure 1: Lumbar spondylolisthesis region

Spondylolisthesis diagnosis requires radiological images produced by using Magnetic Resonance Images (MRI), Computer Tomography (CT), and X-ray radiography technologies [7]. But the identification is commonly done qualitatively in today's clinical practice. Although Meyerding grading provides for a better quantitative assessment of spondylolisthesis, it still relies on time-consuming and inaccurate physical measurements [8].

A CT scan and an MRI require an expert person but an X-ray can be done by a technician, and it is also the first line of investigation [9,10], i.e., before proceeding with any investigation, the doctor prescribed X-ray first. If there is any doubt about in X-rays, then only CT or MRI scans are prescribed. These scans are not easily available in rural areas and very costly [11,12].

Modern healthcare systems make extensive use of Machine Learning (ML) technology for automated solutions that may improve the accuracy and repeatability of crucial job execution [13,14]. The Deep Learning (DL) model learns features from pictures in datasets rather than from explicit programs that must be written for each task [15]. It integrates computational statistics and data mining techniques. DL focuses on teaching computers to learn from data in the same way that humans learn from experiences [16,17].

Multidisciplinary collaboration in technology has produced unique DL models with significant potential and good results to study spondylolisthesis related concerns. A Computer Automated Diagnosis (CAD) system can interpret the number of cases immediately, and reproducible results can be generated using them. This makes an automated spondylolisthesis diagnostic technique appealing for treatment planning and follow-up This mechanism is greatly increasing measurement effectiveness [18].

Convolutional Neural Networks (CNNs) are best suited for image classification tasks. Due to CNN's strength in recording structure and spatial information, it is used for medical images. Visual Geometry Group (VGG) is a well-known tool of CNN for resolving medical image categorization challenges. It is a strong model having a two-dimensional (2D) architecture for feature detection at different positions on targeted images. The transfer learning feature of these models made them popular among researchers. It requires less training, and modification and needs less time to produce results. It is seen in many studies that VGG has achieved results with remarkable accuracy.

Out of various variants of VGG-Net, VGG-16, and VGG-19 were the best performing models, and made public. A few models (MobileNet and ResNets) had many parameters and required a huge number of training images. When evaluated against the VGG16 model, the MobileNet and ResNets models were unable to match the accuracy it provided. It proves the superiority of the VGG16 model over other models. Even though VGG16 is ideally adapted for visual categorization but it has the following constraints:

- VGG16 lost the entity's positional information while max pooling. It ignores a few local structures between simpler objects. However, due to down sampling, VGG16 has some limitations in terms of view invariance and information loss.
- For rotated, tilted, or other abnormal image orientations, VGG16 performs poorly.
- VGG16 proved to be time-consuming as well as requiring a lot of computing resources.

This raises issues related to developing improved disease detection techniques. Capsule network (also known as CapsNet) [19] is one of the most advanced algorithms to resolve these logical restrictions in terms of its generative and deterministic characteristics. CapsNet algorithm uses vectors, which makes it more image-sensitive than the VGG16 that had previously been used. It is a novel approach for capturing the properties and spatial relationships of features in images that has shown promise in image classification [20,21]. Multiple convolutional layers are squashed into capsules by these networks, which are subsequently exposed to nonlinearity.

Vector-based models perform poorly at getting features from images. The original capsule network is inadequate for the classification tasks that involve sophisticated internal representations. To resolve these issues, an integrated model (a combination of VGG16 and CapsNet) named S-VCNet is proposed to predict lumbar spondylolisthesis in X-ray images with better accuracy and loss minimization [22,23].

The proposed model is deployed to the Gradio web app for real time diagnosis of the disease. Furthermore, the results obtained were compared to radiologists' manual observations. This finding directs doctors and practitioners in the proper direction for disease prediction, which can protect many susceptible people and reduce disease rates.

The following are the key goals of this paper:

- To evaluate the performance of VGG16 for lumbar spondylolisthesis diagnosis.
- To design and implement a novel hybrid model (S-VCNet) and compare its performance with VGG16.
- To implement a Gradio-based web interface for real-time diagnosis of lumbar spondylolisthesis quickly and accurately.

The subsection of article include: A review of previously available work is discussed in Section 2, model architecture is described in Section 3, details of the dataset used and the applied methodology are discussed in Section 4, result analysis and discussion are covered in Section 5, and a conclusion is given in Section 6.

2 Literature Review

This section discusses the methods used by various practitioners to identify the existence of medical disease in humans based on X-ray radiographs.

Tiwari et al. [24] have proposed the VGG-CapsNet model for COVID-19 detection in x-ray images. Experimental results suggest that VGG-CapsNet outperforms CapsNet. By integrating CNN with CapsNet, the authors overcome the problems in CNN-based decision support.

Mittal et al. [25] developed two models by integrating “convolutions with capsules” and “ensemble convolutions with capsules” for pneumonia detection using x-ray radiographs. The models have achieved a good accuracy rate.

Yousra et al. [26] presented a useful image categorization model for chest X-rays (CNN-CapsNet). Where feature extractor VGG19 was completely trained on the ImageNet dataset, and the output is passed to CapsNet’s initial feature maps to get the final classification result.

Bharati et al. [27] developed a novel integrated model (VGG + data augmentation + spatial transformer network) with CNN for lung disease diagnosis. According to the findings of this study, the integrated model takes less training time and outperforms the standalone model.

DRISTI (Diabetic Retinopathy classIfication by analyzing reTinal Images) is a study that proposes a hybrid model containing VGG16 and CapsNet to classify diabetic retinopathy. This model is developed for the detection of visual loss earlier and timely treatment of the disease [28].

Nguyen et al. [29] have compared various methods for colorectal tissue classification. The soft voting ensemble model, which included one VGG and one CapsNet model, outperformed independent or ensemble learning with a single base estimator. A hybrid capsule network was created by Boaro et al. [30] for the identification of malignancy in medical images. The VGG16 and a capsule network are coupled in the suggested design. When compared to the literature, the results produced by the suggested model were positive.

Gunasinghe et al. [31] have developed a model utilizing CNN with CapsNet to diagnose lung disorders, including combining patient information with data from chest X-rays. Toraman et al. [32] presented the difficulties in recognizing COVID-19 owing to symptoms that are similar to those of lung infections. The authors used CapsNet to create a system that was trained and evaluated for pneumonia patients.

Saif et al. [33] introduced CapsNet for musculoskeletal radiograph anomaly identification, and it has been shown that its architecture has very promising features that can assist in solving CNN’s limitations. Singh et al. [34] have proposed a method for glaucoma prediction in images using both early and late fusion. They have successfully implemented fusion based on features and image levels.

For the identification of COVID-19, Aksoy et al. [35] developed a capsule network on a cloud platform for quicker and easier processing. Abdollahi et al. [36] have applied the VGG16 model for epidemic-type identification in chest x-ray radiographs.

Sharma et al. [37] have used CapsNet with shallow architecture for COVID-19 diagnosis. They have used 5 fold-cross validation technique on the dataset having multiclass classification.

Qiu et al. [38] have developed several novel model architectures by combining various CNN models with CapsNet. The proposed models have achieved accuracy ranges from 95% to 98% for COVID-19 detection in both multi-class and binary classification.

Table 1 summarizes the literature and indicates that integrated models are used in different application fields specifically for disease detection. But very little work has been done for lumbar spondylolisthesis diagnosis and there is scope for improving accuracy and making models generalize. So, the study proposed an integrated deep learning-based web interface to diagnose lumbar spondylolisthesis.

Table 1: Literature review summary

Source	Purpose	Major findings	Accuracy
Tiwari et al. [24]	COVID-19 detection	VGG-CapsNet can eliminate faults in the CNN model DSS for COVID-19 detection.	97%
Mittal et al. [25]	Detection of pneumonia	An integrated model is used for pneumonia detection in radiographs.	95.33%
Yousra et al. [26]	Image classification	VGG19 and CapsNet are combined to overcome their drawbacks.	94%
Bharati et al. [27]	Detection of Lung disease	An integrated model VDSNet is proposed for disease detection.	73%
Kumar et al. [28]	Diagnosis of diabetic retinopathy	An integrated model is proposed to classify diabetic retinopathy.	5-classes: 82% 2-classes: 96%
Nguyen et al. [29]	Colorectal tissue classification	"Soft Voting," a hybrid model is proposed for disease diagnosis.	93%–98% for all classes
Boaro et al. [30]	Detection of melanoma	VGG16 was combined with a capsule neural network to observe the structures of the skin.	92.6%

(Continued)

Table 1: Continued

Source	Purpose	Major findings	Accuracy
Gunasinghe et al. [31]	Prediction of Lung Diseases	CNN is combined with CapsNet to identify lung diseases.	–
Toraman et al. [32]	COVID-19 Detection	With binary classification and multi-class classification, the suggested technique is meant to deliver rapid and accurate diagnoses for COVID-19 disorders.	97.24%
Saif et al. [33]	Musculoskeletal abnormality detection	A CapsNet architecture is proposed to overcome CNN's limitations.	95.15%
Singh and Khanna [34]	Glaucoma prediction	Feature and image level glaucoma prediction	95.56%
Aksoy et al. [35]	COVID–19 detections	Proposed cloud computing-based capsule network for disease detection.	98%
Abdollahi et al. [36]	Epidemic types	Proposed a powerful model for disease detection.	97%
Sharma et al. [37]	COVID-19 detection out of 3 classes	Integrated model outperforms a single model.	96.47%
Qiu et al. [38]	COVID-19 detection	For the binary and multiclass classifications, the novel hybrid models were applied.	95–98%

3 Model Architecture

3.1 VGG-Net Architecture

VGG-Net is a widely used CNN architecture that gains popularity due to its outstanding performance on the ImageNet dataset. TheVGG16 architecture works well with various datasets; therefore, it was chosen for this study. It consists of convolutional layers, ReLU (activation function), pooling layers, and fully connected layers. In input, a 2D convolutional layer with 3 × 3 convolutional filters was used. Images (reduced to the size of 224 × 224 pixels) are fed to the first convolution layer for detecting low-level features. It contains position definitions for lines and edge points.

An activation function (ReLU) along with max pooling is applied to all hidden layers. It uses the pixel positions for generating the feature map. This is a high-level feature used for sharing weights to reduce unnecessary or redundant load. Image area is reduced by combining a few neurons by using the pooling technique. At last, three fully connected layers were used, which contain the SoftMax function for classification tasks. VGG Net's architecture is depicted in Fig. 2.

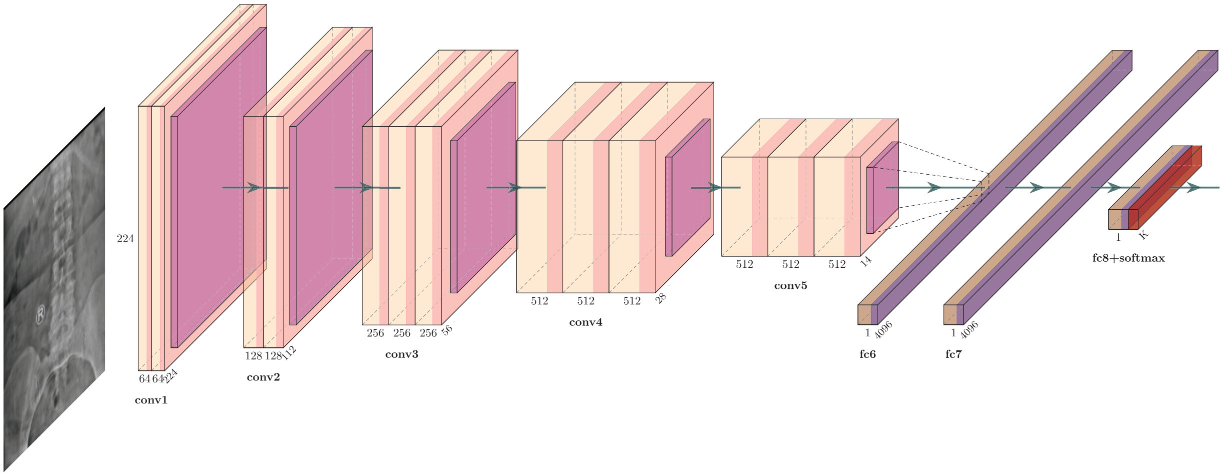

Figure 2: VGG16 model architecture for lumbar spondylolisthesis prediction

3.2 CapsNet Architecture

Deep models commonly encode the entities with vectors. However, this concept is rarely applied to image categorization. The capsule networks (CapsNets) use "vector-wise" encoding, in which items are encoded by capsules (groups of neurons). It helps in fixing the position of objects and managing the relationship between them. It overcomes the problem of information loss caused by pooling layers in CNN, such as location, size, rotation, and scale, as described in Fig. 3.

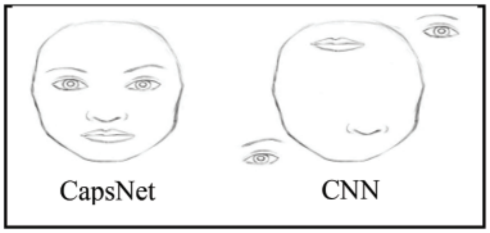

Figure 3: CapsNet *vs*. CNN Model

A capsule is made up of a pose vector or matrix for encoding the object's instantiation of various layers parameters and an activation. The instantiation parameters change as the viewing circumstances change, but the capsule remains active. With the ability to assign parts to wholes, equivariance, and invariance are two qualities that are utilized to build visual hierarchical connections.

CapsNets may simulate visual hierarchical relationships due to the "Dynamic routing" method [39]. In CapsNets, dynamic routing is used to establish visual hierarchical relationships via a method called "routing-by-agreement" to repeatedly route information transitioning from lower to higher level capsules, which is the key concept of dynamic routing in CapsNets.

Fig. 4 depicts the CapsNet architecture for spine x-ray image classification. In this first layer, the ReLU function is activated with 256 filters and takes the parameter of size 9 × 9 with stride one. Features are passed to the primary capsules through this function.

3.2.1 CapsNet's Basic Mathematics

CapsNet employed three unique mechanisms:

- Convolution,
- Reshaping function, and
- Squash function.

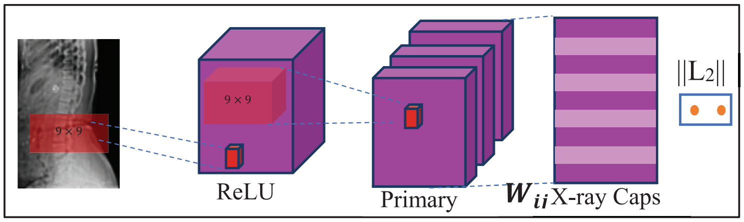

Figure 4: CapsNet architecture for spine x-ray diagnosis

The input is given to the convolutional layers in the convolution process that is used to generate a list of "feature maps". These feature maps are now reshaped using the Reshaping function. Finally, each vector's length is kept inside the range of 1 and 0, according to the squash function. Because it represents the probability that an item will be found at a specific spot in the image and it does not cause the positional data contained in a high-dimensional vector to be destroyed [40].

Assume that layer l and layer $l+1$ have m and n capsules, respectively. We must compute the activations of the capsules at layer $l+1$ based on the activations at layer l. The letter u is used to represent capsule activations at layer l. We must compute v, the capsule activations, at layer $l+1$.

For a capsule j at layer $l+1$,

1. At layer l, the capsules are used to calculate the prediction vectors. The prediction vector (shown in equation 1) for the capsule j (of layer $l+1$) generated by capsule i (of layer l) is:
$$u_{j|i} = W_{ij}u_i \tag{1}$$
W_{ij} represents "weight matrix".
2. Now the output vector for capsule j is calculated (in Eq. (2)). The output vector for capsule j is the sum of the weights of all the prediction vectors supplied by layer l capsules:
$$s_j = \sum_{i=1}^{m} c_{ij}u_{j|i} \tag{2}$$
3. Scalar c_{ij} represents the coupling coefficient between capsules i (of layer l) and j (of layer $l+1$). A method called the iterative dynamic routing algorithm determines these coefficients.
4. To obtain the activation v_j of the capsule j, we apply the squashing function (shown in Eq. (3)) to the output vector:
$$v_j = squash(s_j) \tag{3}$$
5. Long vectors are pushed toward 1 and shot vectors are pushed toward 0 by the squashing function.

3.2.2 Dynamic Routing Algorithm

Dynamic Routing Algorithm is more efficient than max pooling. It gives solid support to those capsules that have reached the parent output. It provides a non-linear relationship by using mathematical concepts explained in the earlier section. It is generally applicable to scalar values.

The layer $l+1$ activation vectors transmit feedback signals to the layer l capsules. The dot product should be high if the prediction vector of capsule i (of layer l) for capsule j (of layer $l+1$) agrees with the activation vector of capsule j. As a result, the "weight" of the prediction vector $u_{j|i}$ in the output vector of j is raised. Simply, the output vector gives a lot more weight to those prediction vectors that assisted the activation vector (and consequently the activation vector). For $4-5$ cycles, this circle of reciprocal assistance continues.

The predictions for high-level capsules from a low-level capsule should add up to one (i.e., $\sum_k c_{ik} = 1$). As a result, capsule i (of layer l),

$$c_{ij} = \frac{exp(b_{ij})}{\sum_k exp(b_{ik})} \tag{4}$$

The b_{ij} (initially equals to one) reveals how closely capsules i (of layer l) and j (of layer $l+1$) are linked. Eq. (4) illustrates a measure of the number of capsules i which explains the presence of the capsule j.

Algorithm 1: Routing Algorithm

```
Given: Prediction vectors $u_{j|i}$ number of routing iterations $r$
∀ capsule $i$ in layer $l$ and capsule $j$ in layer $l+1$: $b_{ij} = 0$
for $r$ iterations do:
    for ∀ capsules $i$ in the layer $l$: $c_i = softmax(b_i)$ (A capsule's bets on high-level capsules should equal to 1)
    for ∀ capsules $j$ in the layer $l$+1: $s_j = \sum_{i=1}^{m} c_{ij} u_{j|i}$ (output vector is a weighted sum of prediction vectors)
    for ∀ capsules $j$ in the layer $l+1$: $\mathrm{v_j} = \mathrm{squash}(s_j)$ (apply activation function)
    for ∀ capsule $i$ in layer $l$ and capsule $j$ in layer $l+1$: $b_{ij} = b_{ij} + u_{j|i} \cdot v_j$
return $v_j$
```

The routing takes place at the last line of the loop. If the product $u_{j|i} \cdot v_j$ is big, it will raise b_{ij}, which will increase the associated coupling coefficient c_{ij}, causing the product $u_{j|i} \cdot v_j$ to grow more.

3.3 Proposed Model Architecture

Transfer learning technique is used as a preliminary step for a few tasks. Utilizing knowledge from other areas to improve the quality of learning in the actual environment is the aim of transfer learning.

Reducing the amount of training time is possible through transfer learning. This approach could be connected to the creation of deep learning visual categorization models. A deep CNN and a smaller kernel size can improve model performance, as demonstrated by VGG16. As a result, the VGG16 architecture of CNN has been proposed as an integrated with CapsNet for faster processing. As a mixture of these two powerful architectures, the VGG16 is used to replace the feature extraction section of CapsNet in the research work. Fig. 5 shows the proposed integrated model architecture that includes a two-stage recommended paradigm.

The base network architecture is the VGG16 network with 2D kernels. In the first phase, Initial feature maps are derived from a spine X-ray radiograph using a VGG16 model. Conv1 kernels in VGG16 have been modified to support x-ray radiographs. VGG16 is invariant as a result of the pooling procedure, the model is reduced at the block 5 pool. After block5_pool, the capsule network is combined with VGG16. This upgradation can be considered as transfer learning and its goal is to utilize the feature extraction capability and pass it to CapsNet. So, CapsNet may properly identify the low-level feature.

In the second phase, the features hierarchy is encoded to multi-dimensional main capsules via the global average-pooling layer. The pooling layer in VGG16 selects the backward-transmitted input and transfers the parameters between the two convolutional layers. CapsNet minimizes this marginal loss by dynamically adjusting the network's parameters. For binary class prediction tasks, the lambda function is used.

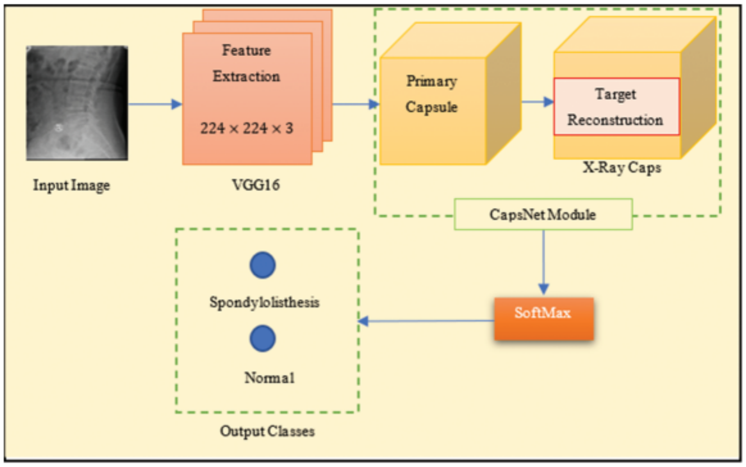

Figure 5: Integrated model (S-VCNet) architecture

4 Experimental Set-Up

The experiment was performed on programming language "Python3" by using Google Colab IDE. The Keras and TensorFlow frameworks were used as a feature extractor, and for scientific computing, various open-source libraries such as Pandas, NumPy, and Scikit-learn were applied. Pyplot module from the matplotlib package is utilized for accuracy and loss curve visualization.

4.1 Image Acquisition

A private dataset of 466 spinal x-ray radiographs was used in this investigation. There are 186 images of the patient with spondylolisthesis, compared to 280 images of the healthy patient. The images were converted into 224 × 224 pixels. Fig. 6 displays a few pictures of patients with normal and spondylolisthesis cases from the dataset.

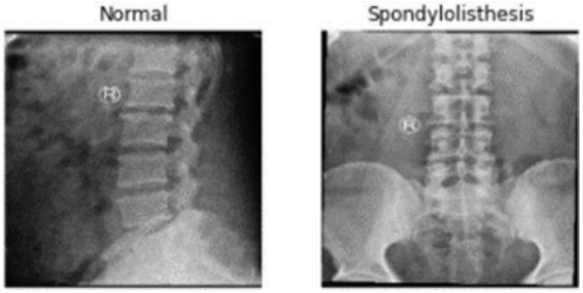

Figure 6: X-ray Radiographs from dataset

4.2 Data Splitting

Collected data is split into two parts: training data, and testing data. A balanced set of images were selected from each category of image. A total of 343 samples are used to train the model. For performance checking, 123 images are randomly selected from the total sample. A quantitative breakdown of data splitting is shown in Table 2.

Table 2: Statistics after data splitting

Test type	Training data	Testing data	Total
Healthy	220	60	280
Diseased	123	63	186
Total	343	123	466

4.3 Training and Optimization

The foundational network design was provided by the VGG16 network with 2D kernels, and it has utilized a fixed image size of 224 × 224. The Conv1 kernels of VGG16 have been modified to accept the input. After block5_pool was reached, the capsule network was combined with VGG16. For binary class prediction tasks, a lambda function was utilized. The overall model contains a total of 21 M trainable parameters. Out of those 13 M parameters are trainable and 7 M parameters are non-trainable. The pre-trained ImageNet weights are used to train all the tasks end-to-end simultaneously using an 'Adam' optimizer. It is a simple and computationally efficient gradient-based loss function optimization technique. The loss function's objective during training is to reduce the model's loss. Loss is defined as the discrepancy between the expected and actual value.

A loss function, namely categorical cross entropy, is used to find the variation between two quantities. It is a strengthening tool that can differentiate the given quantities. An example is given below, in Table 3, to understand this example a bit more. Suppose we take the first case where:

Door 3 shows the negative likelihood or 1, the probability that is the probability of not getting a gift. Here, y shows the number of gifts is behind the door. Categorical cross-entropy (CCE) can be formulated as follows,

$$CCE = -\frac{1}{N}\sum_{i=1}^{N}\sum_{c=1}^{C} y_c.log(\hat{y}_c) + (1 - y_c) \,.\, \log(1 - \hat{y}_c) \tag{5}$$

Table 3: Example of categorical cross entropy

Door 1	Door 2	Door 3
p(gift) $= \hat{y}_c = 0.8$	p(gift) $= \hat{y}_c = 0.7$	p(gift) $= \hat{y}_c = 0.1$ OR 1-p(gift) $= 1 - \hat{y}_c = 0.9$
y = 1	y = 1	y = 0

For the given example, the above formula is used to calculate entropy. The cross-entropy is calculated by the negative logarithm. It is allowed for the two functions, y_c, and $\hat{y}_c$. Where the groundtruth and predicted values of the image object are represented by y_c and $\hat{y}_c$, respectively. C indicates the number of classes and N indicates the number of observations. Cross-entropy is generally used to describe the closeness between the predicted distribution and the actual distribution. The minus sign ensures that the loss gets smaller when the measurements get closer to each other. A SoftMax activation function is used in conjunction with the CCE cost function. It is used to calculate the loss between predicted and target values in multi-class classification. The pre-trained ImageNet weights are used to train all the tasks end-to-end simultaneously using an optimizer.

The goal of the Adam optimizer is to minimize the *loss* function. It is a method of calculating current gradients using prior gradients. Adam is a hybrid combination of the AdaGrad and RMSProp methods. Adam also applies the concept of momentum to the current gradient by combining fractions of prior gradients. This optimizer has gained a lot of popularity and is now widely used in neural network training.

Adam uses two moments in the gradients: variable v_t as the first moment (the mean) and variable s_t as the second moment (the uncentered variance). The Adam estimator can be generated using the hyper parameters $0 \leq \beta_1, \beta_2 < 1$, and an Exponentially Weighted Moving Average (EWMA) as follows [41].

Algorithm 2: Adam Estimator

```
1   Initialize: $\beta_1\beta_2\epsilon\,[0,1]\,, v_0, s_0$, learning rate $\eta$, and stochastic objective function $f(x_t)$ with
    parameters $x_t$.
2   Find $f(x_t)$ using the formula: $g_t = \nabla_x f_t(x_{t-1})$.
    Update moments (1st & 2nd) using the below formula:
3       $v_t = \beta_1 v_{t-1} + (1 - \beta_1)\, g_t$
$s_t = \beta_2 s_{t-1} + (1 - \beta_2)\, g_t \odot g_t$
    Find the corrected bias:
4   $\hat{v}_t = \frac{v_t}{1 - \beta_1^t}$,
    $\hat{s}_t = \frac{s_t}{1 - \beta_2^t}$ .
    Corrected bias parameters were used to modify the learning rate of each model parameter:
5   $\grave{g}_t = \frac{\eta \hat{v}_t}{\sqrt{\hat{s}_t} + \varepsilon}$ , (where $\eta$ denotes the learning rate and $\varepsilon = 10^{-8}$ denotes the error criteria)
6   Modify $x_t$ as: $x_t = x_{t-1} - \grave{g}_t)$
7   Repeat steps 2 to 6 until the parameter $x_t$ converges.
```

Adam used stochastic gradient descent to keep all weight updates and assured that the learning rate remains constant throughout the training. Each network weight (parameter) has its learning rate, which is maintained and changed as learning progresses. In addition, the algorithm computes an exponential moving average of the gradient as well as the squared gradient, with hyper parameters β_1 and β_2 controlling the decay rates. The learning rate is set to $\eta = 0.0001$, $\beta_1 = 0.9$, and $\beta_2 = 0.999$ in the initialization.

4.4 Performance Evaluation Tools

The effectiveness of any DL model is defined by several performance assessment measures in the field of soft computing. The selection of metrics is decided according to the task handled. The current study is concerned with image classification tasks, therefore, the accuracy/loss graph, confusion matrix etc. are used as performance assessment metrics. Loss and accuracy will be used to assess model performance in this investigation. A confusion matrix is a much better approach to assessing a classifier's performance in a classification problem for determining the model's accuracy and precision. It works for both binary and multi-class classification systems.

A confusion matrix is not a performance metric itself, but it does allow for the computation of certain useful performance measures based on the true positive (TP), false positive (FP), false negative (FN), and true negative (TN) values. The words TP, FP, FN, and TN have been described below in the context of the considered situation:

- **TP:** A case is true positive if the patient has spondylolisthesis (class 1) and the classifying model predicted the case to be spondylolisthesis as well (class 1).
- **FP:** It has occurred when a patient with a healthy spine (class 0) is diagnosed with spondylolisthesis (class 1).
- **FN:** It is the reverse of FP, in which a patient with spondylolisthesis (class 1) is anticipated as healthy (class 0).
- **TN:** If a patient has a healthy spine (class 0) and is also predicted as healthy (class 0), the situation falls into the TN category.

For performance assessment, all the samples were observed from training and test categories. Some useful parameters for performance measures are computed using the confusion matrix. These metrics can be defined as follows:

Accuracy: This term is described by the number of right predictions divided by the total number of predictions.

$$Accuracy = \frac{Correctlyclassifiedimages}{Totalnumberofimages} = \frac{(TP + TN)}{(TP + FP + TN + FN)} \tag{6}$$

Precision: Precision is a metric for determining the accuracy of a prediction.

$$Pricision = \frac{Imagescorrectlyclassifiedasn}{Imagesclassifiedasn} = \frac{TP}{(TP + FP)} \tag{7}$$

Recall: Recall is the measure of successful identification of the ground truth.

$$Recall = \frac{Imagescorrectlyclassifiedasn}{Imagesofclassn} = \frac{TP}{(TP + FN)} \tag{8}$$

F1 Score: The F1 score is calculated using the harmonic mean of precision and recall.

$$F_1 ScoreorF_{avg} = 2*\frac{(Precision*Recall)}{(Precision + Recall)} \tag{9}$$

Sensitivity (SN): This term is described by the number of correct positive predictions divided by the total number of positive predictions.

$$Sensitivity = \frac{TP}{(TP + FN)} \tag{10}$$

Specificity (SP): This term is described by the number of correct negative predictions divided by the total number of negative predictions.

$$Specificity = \frac{TN}{(TN + FP)} \tag{11}$$

5 Result Analysis

5.1 Experimental Results

Confusion metrics were used to evaluate the prediction ability of developed models. To reduce over fitting and increase training data artificially, data augmentation techniques such as rotation, flipping, and zooming were used in this study. The history object was used to collect metric values for performance measurement during training. Continued learning of the VGG16 and S-VCNet is visualized using an accuracy/loss graph shown in Figs. 7 and 8, respectively.

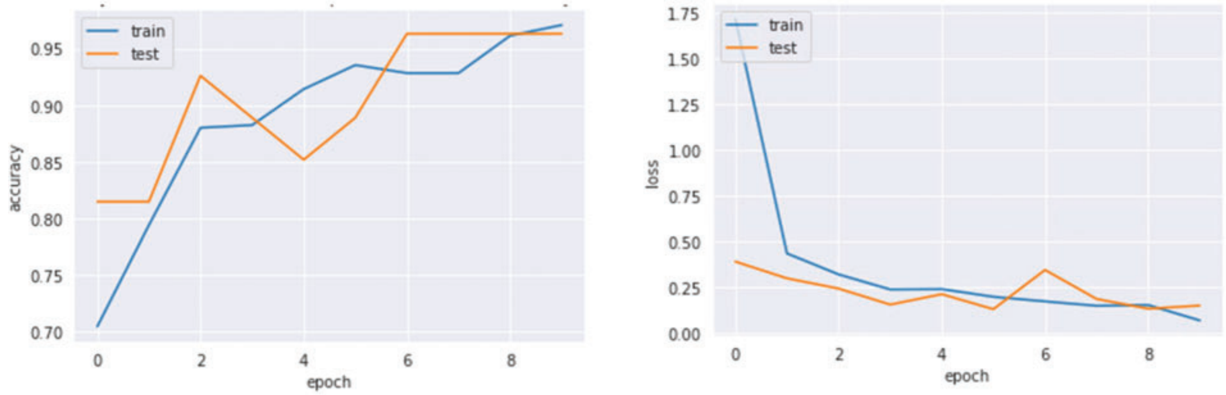

(a) VGG16's Training Accuracy (b) VGG16's Training Loss

Figure 7: VGG16's performance graph

The confusion matrix of selected models was displayed in Fig. 9 Actual instances were grouped in rows in the confusion matrix, whereas expected cases were grouped in columns and denoted as normal and spondylolisthesis cases.

The test set included a total of 123 X-ray radiographs (63 for spondylolisthesis and 60 for normal). Table 4 lists the performance metrics of the VGG16 and VGG-CapsNet classifiers for each class (Spondylolisthesis *vs*. Normal).

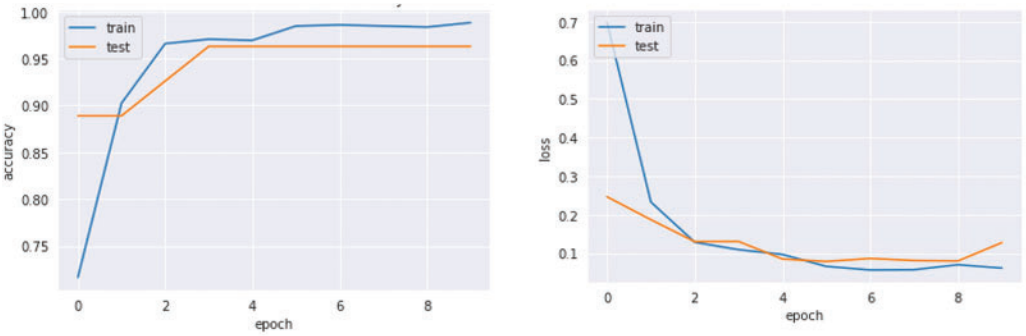

(a) S-VCNet's Training Accuracy (b) S-VCNet's Training Loss

Figure 8: S-VCNet's performance graph

The above table shows that models have learned effectively. VGG16 has achieved 95% accuracy by misclassifying only 1 case as normal and 5 cases as spondylolisthesis. The suggested integrated model has achieved 98% accuracy by misclassifying only 1 case as normal and 2 cases as spondylolisthesis. The training loss of VGG16 and the integrated model are recorded as 0.23 and 0.08, respectively. After the result analysis, it is confirmed, the S-VCNet model outperformed for the spondylolisthesis detection.

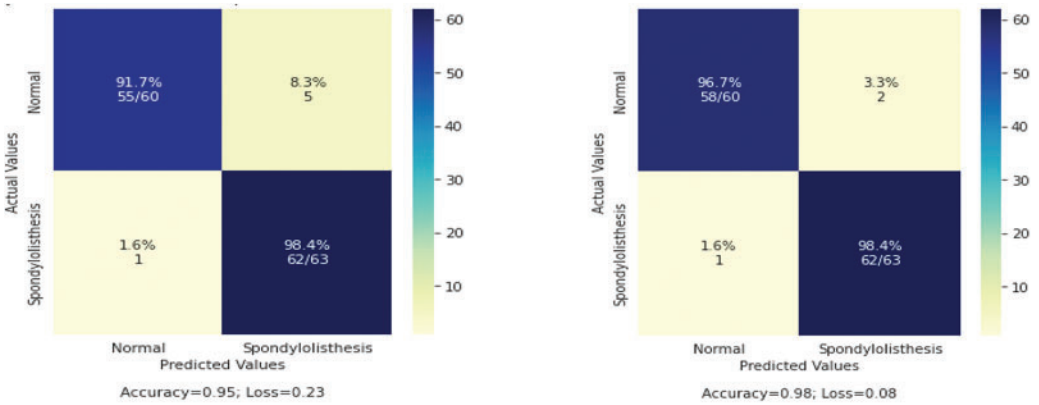

(a) VGG16's confusion matrix (b) S-VCNet's confusion matrix

Figure 9: Confusion matrix of VGG16 and S-VCNet

Table 4: Performance assessment of classification models

Model	Class	Performance metrics						
		Accuracy	Precision	Recall	$F1$-score	Loss	SP	SN
VGG 16	Normal	0.95	0.98	0.92	0.95	0.23	0.93	0.98
	Spondylolisthesis		0.93	0.98	0.95			
S-VCNet	Normal	0.98	0.98	0.97	0.97	0.08	0.97	0.98
	Spondylolisthesis		0.97	0.98	0.98			

5.2 Gradio Implementation

The architecture of Gradio is based on a client-server model, where the client is a web browser and the server is a Python-based web application. While creating the Gradio interface a Python function needs to be defined that takes input from the user and returns an output. Then it generates a web page that allows users to interact with functions through a web form. After form submission the input is sent to the server, which runs those functions and returns the output to the user's browser [42].

Gradio uses Flask, a lightweight web framework, as its server technology. It handles the HTTP requests and responses and provides a simple way to create routes that map to your Python functions. Gradio also uses Socket.IO to handle real-time communication between the client and server, allowing for a smooth and responsive user experience.

Under the hood, Gradio uses JavaScript and CSS to create the user interface, and it includes several pre-built components that you can use to customize your interface. Gradio also supports a wide variety of input and output types, including images, text, audio, and video. Overall, the architecture of Gradio is designed to be simple and flexible, allowing you to quickly create and deploy web interfaces for your ML models with minimal overhead [43].

After testing the integrated model, it is used as a web app for Lumbar Spondylolisthesis diagnosis on the Gradio platform. To access this application, the patient must first complete a hospital-based spine X-ray screening. Take a photo of the X-ray film and upload it using the "Drop Image Here or Click to Upload", then hit the Submit button. Finally, spondylolisthesis may be detected using the Gradio platform.

Fig. 10 illustrates that the Gradio-based tool successfully recognized normal and spondylolisthesis cases within 20 s. The probability of the two classes will be presented as a percentage after hitting the Submit button (as shown in Figs. 10a and 10b). The X-ray image of the spine will most likely fall into one of two categories.

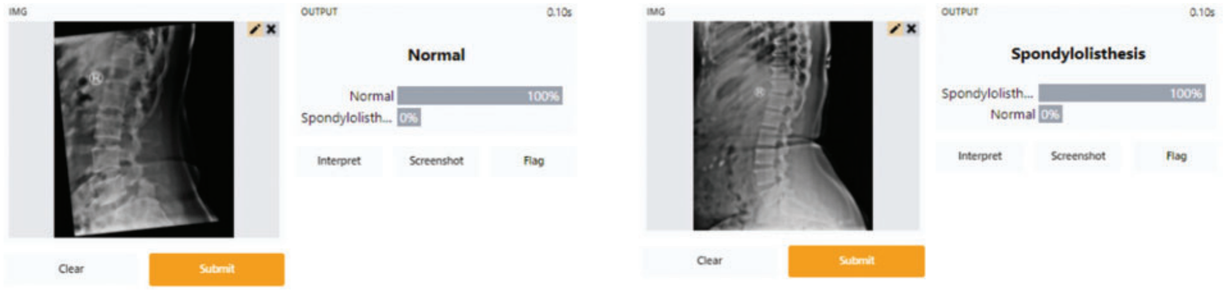

(a) recognized normal case

(b) recognized spondylolisthesis case

Figure 10: Screenshots of the gradio web application tool

6 Discussion

The suggested model, S-VCNet, is found to take less time to diagnose lumbar spondylolisthesis and have high sensitivity and specificity, as shown by the figures and tables presented above. The model could be utilized in building a real-time diagnostic system for routine clinical practice. The results produced by VGG16 alone are not that beneficial, but the transferred weights from VGG16 to CapsNet for the classification task are found to be beneficial. The ultimate objective of the model is to minimize marginal loss for accurate and swift diagnosis, which was discovered to be significantly better than training the CapsNet from scratch. Compared to previous studies on integrated CapsNet models by Tiwari et al. [24], Kumar et al. [28], and Bharati et al. [27], the proposed model in this study achieved a peak accuracy of 98%.

7 Conclusion

In this study, a novel integrated model called "S-VCNet" is created using a web application for the prediction of Lumbar Spondylolisthesis, as an alternative to manual radiological examination. The suggested model improved the performance of the VGG16 model by utilizing the initial feature map. Comparative experiments demonstrated that the overall performance of S-VCNet was superior to previously created models. However, the model had significant limitations in accurately classifying some spondylolisthesis positive cases as negative or vice versa, indicating the need for further research in the diagnosis of lumbar spondylolisthesis. Although this study provides a foundation for predicting lumbar spondylolisthesis, grading the spondylolisthesis is important. Therefore, future studies should focus on (1) improving this algorithm for lumbar spondylolisthesis grading, and (2) developing a mobile app for the disease identification.

Acknowledgement: No grant is received for this paper from any funding organization.

Funding Statement: The authors received no funding for this study.

Conflicts of Interest: The authors declare that they have no conflicts of interest to report regarding the present study.

References

[1] R. V. Johny and R. Roseline Mary, "Classification and correlational analysis on lower spine parametersusing data mining techniques," *International Journal of Recent Technology and Engineering*, vol. 7, no. 6, pp. 1450–1456, 2019.

[2] L. Kalichman and D. J. Hunter, "Diagnosis and conservative management of degenerative lumbar spondylolisthesis," *European Spine Journal*, vol. 17, no. 3, pp. 327–335, 2008. https://doi.org/10.1007/s00586-007-0543-3

[3] S. Tenny and C. C. Gillis, "Spondylolisthesis," in *The Growing Spine: Management of Spinal Disorders in Young Children*, Second ed., pp. 415–448, 2017. Accessed: Oct. 11, 2021, http://europepmc.org/books/NBK430767

[4] N. Ebraheim, H. Elgafy, P. Gagnet, K. Andrews and K. Kern, "Spondylolysis and spondylolisthesis: A review of the literature," *Journal of Orthopaedics*, vol. 15, no. 2, pp. 404–407, 2018. https://doi.org/10.1016/j.jor.2018.03.008

[5] F. Varcin, H. Erbay, E. Cetin, I. Cetin and T. Kultur, "Diagnosis of lumbar spondylolisthesis via convolutional neural networks," in *Proc. 2019 Int. Conf. on Artificial Intelligence and Data Processing Symp. (IDAP)*, Malatya, Turkey, pp. 1–4, 2019. https://doi.org/10.1109/IDAP.2019.8875988

[6] V. M. Ravindra, S. S. Senglaub, A. Rattani, M. C. Dewan, R. Härtl *et al., Degenerative lumbar spine disease: Estimating global incidence and worldwide volume*, Los Angeles, CA: SAGE Publications, 2018.

[7] A. Jamaludin, *Automated analysis of spinal MRI using deep learning*, England: University of Oxford, 2017.

[8] S. Liao, Y. Zhan, Z. Dong, R. Yan, L. Gong *et al.,* "Automatic lumbar spondylolisthesis measurement in CT images," *IEEE Transactions on Medical Imaging*, vol. 35, no. 7, pp. 1658–1669, 2016. https://doi.org/10.1109/TMI.2016.2523452

[9] L. Saba, M. Biswas, V. Kuppili, E. C. Godia, H. S. Suri *et al.,* "The present and future of deep learning in radiology," *European Journal of Radiology*, vol. 114, no. February, pp. 14–24, 2019. https://doi.org/10.1016/j.ejrad.2019.02.038

[10] K. Singh, B. Sharma, J. Singh, G. Srivastava, S. Sharma *et al.,* "Local statistics-based speckle reducing bilateral filter for medical ultrasound images," *Mobile Networks and Applications*, vol. 25, pp. 2367–2389, 2020.

[11] D. Koundal, B. Sharma and Y. Guo, "Intuitionistic based segmentation of thyroid nodules in ultrasound images," *Computers in Biology and Medicine*, vol. 121, pp. 103776, 2020.

[12] S. Jalal, W. Parker, D. Ferguson and S. Nicolaou, "Exploring the role of artificial intelligence in an emergency and trauma radiology department," *Canadian Association of Radiologists Journal*, vol. 72, no. 1, pp. 167–174, 2021. https://doi.org/10.1177/0846537120918338

[13] D. Saravagi, S. Agrawal and M. Saravagi, "Opportunities and challenges of machine learning models for prediction and diagnosis of spondylolisthesis: A systematic review," *International Journal of Engineering Systems Modelling and Simulation*, vol. 12, no. 2–3, pp. 127–138, 2021. https://doi.org/10.1504/IJESMS.2021.115534

[14] Z. Ahmed, K. Mohamed, S. Zeeshan and X. Dong, "Artificial intelligence with multi-functional machine learning platform development for better healthcare and precision medicine," *Database*, vol. 2020, no. 104, pp. 23, 2020. https://doi.org/10.1093/database/baaa010

[15] M. Sethi, S. Ahuja and V. Kukreja, "An empirical study for the deep learning models," *Journal of Physics: Conference Series*, vol. 1950, no. 1, pp. 012071, 2021. https://doi.org/10.1088/1742-6596/1950/1/012071

[16] M. Agrawal and S. Agrawal, "A systematic review on artificial intelligence/deep learning applications and challenges to battle against covid-19 pandemic," *Disaster Advances*, vol. 14, no. 8, pp. 90–99, 2021. https://doi.org/10.25303/148da9021

[17] R. Tandon, S. Agrawal and P. Goyal, "Sequential convolutional neural network for automatic breast cancer image classification using histopathological images," *Journal of Critical Reviews*, vol. 7, no. 15, pp. 6104–6117, 2020.

[18] D. Saravagi, S. Agrawal, M. Saravagi and M. H. Rahman, "Diagnosis of lumbar pondylolisthesis using a pruned CNN model," *Computational and Mathematical Methods in Medicine*, vol. 2022, no. 6, pp. 1–10, 2022. https://doi.org/10.1155/2022/2722315

[19] S. Sara, F. Nicholas and G. E. Hinton, "Dynamic routing between capsules Advances in Neural Information Processing Systems 30," in *Proc. of the Annual Conf. on Neural Information Processing Systems*, pp. 3856–3866, 2017.

[20] G. Zhao, Y. Wu, M. He, J. Bai, J. Cheng *et al.,* "Preprocessing and grading of glioma data acquired from multicenter," *Journal of Medical Imaging and Health Informatics*, vol. 9, no. 6, pp. 1236–1245, 2019. https://doi.org/10.1166/JMIHI.2019.2724

[21] M. Raghu, C. Zhang, J. Kleinberg and S. Bengio, "Transfusion: Understanding transfer learning for medical imaging," *Advances in Neural Information Processing Systems*, vol. 32, no. NeurIPS, 2019.

[22] V. K. Sakshi and S. Ahuja, "Recognition and classification of mathematical expressions using machine learning and deep learning methods," in *2021 9th Int. Conf. on Reliability, Infocom Technologies and Optimization (Trends and Future Directions), ICRITO 2021*, Noida, pp. 1–5, 2021. https://doi.org/10.1109/ICRITO51393.2021.9596161

[23] D. Saravagi, S. Agrawal, M. Saravagi, J. M. Chatterjee and M. Agarwal, "Diagnosis of lumbar spondylolisthesis using optimized pretrained CNN models," *Computational Intelligence and Neuroscience*, vol. 2022, pp. 1–12, 2022. https://doi.org/10.1155/2022/7459260

[24] S. Tiwari and A. Jain, "Convolutional capsule network for COVID-19 detection using radiography images," *International Journal of Imaging Systems and Technology*, vol. 31, no. 2, pp. 525–539, 2021. https://doi.org/10.1002/IMA.22566

[25] A. Mittal, D. Kumar, M. Mittal, T. Saba, I. Abunadi *et al.,* "Detecting pneumonia using convolutions and dynamic capsule routing for chest X-ray images," *Sensors*, vol. 20, no. 4, pp. 1068, 2020. 10.3390/S20041068

[26] D. Yousra, A. B. Abdelhakim and B. A. Mohamed, “A novel model for detection and classification coronavirus (COVID-19) based on chest x-ray images using CNN-CapsNet,” *Sustainable Smart Cities and Territories*, vol. 253, no. 8, pp. 187–199, 2021. 10.1007/978-3-030-78901-5_17

[27] S. Bharati, P. Podder and M. R. H. Mondal, “Hybrid deep learning for detecting lung diseases from X-ray images,” *Informatics in Medicine Unlocked*, vol. 20, pp. 1–23, 2020. https://doi.org/10.1016/j.imu.2020.100391

[28] G. Kumar, S. Chatterjee and C. Chattopadhyay, “DRISTI: A hybrid deep neural network for diabetic retinopathy diagnosis,” *Signal Image and Video Processing*, vol. 15, no. 8, pp. 1679–1686, 2021. https://doi.org/10.1007/s11760-021-01904-7

[29] H. G. Nguyen, A. Blank, H. E. Dawson, A. Lugli and I. Zlobec, “Classification of colorectal tissue images from high throughput tissue microarrays by ensemble deep learning methods,” *Scientific Reports*, vol. 11, no. 1, pp. 1–11, 2021. https://doi.org/10.1038/s41598-021-81352-y

[30] J. M. C. Boaro, P. T. C. Dos Santos, C. V. M. Rocha, T. Fontenele, G. B. Junior *et al.,* “Hybrid capsule network architecture estimation for melanoma detection,” in *Int. Conf. on Systems, Signals, and Image Processing*, Niteroi, vol. 2020, pp. 93–98, 2020. 10.1109/IWSSIP48289.2020.9145127

[31] A. D. Gunasinghe, A. C. Aponso and H. Thirimanna, “Early prediction of lung diseases,” in *2019 IEEE 5th Int. Conf. for Convergence in Technology, I2CT 2019*, Bombay, pp. 1–4, 2019. 10.1109/I2CT45611.2019.9033668

[32] S. Toraman, T. B. Alakus and I. Turkoglu, “Convolutional capsnet: A novel artificial neural network approach to detect COVID-19 disease from X-ray images using capsule networks,” *Chaos, Solitons, and Fractals*, vol. 140, pp. 110122, 2020. https://doi.org/10.1016/J.CHAOS.2020.110122

[33] A. F. M. Saif, C. Shahnaz, W. P. Zhu and M. O. Ahmad, “Abnormality detection in musculoskeletal radiographs using capsule network,” *IEEE Access*, vol. 7, pp. 81494–81503, 2019. https://doi.org/10.1109/ACCESS.2019.2923008

[34] L. K. Singh and M. Khanna, “A novel multimodality based dual fusion integrated approach for efficient and early prediction of glaucoma,” *Biomedical Signal Processing and Control*, vol. 73, pp. 103468, 2022. https://doi.org/10.1016/j.bspc.2021.103468

[35] B. Aksoy and O. K. M. Salman, “Detection of COVID-19 disease in chest X-ray images with capsul networks: Application with cloud computing,” *Journal of Experimental & Theoretical Artificial Intelligence*, vol. 33, no. 3, pp. 527–541, 2021. https://doi.org/10.1080/0952813X.2021.1908431

[36] J. Abdollahi and L. Mahmoudi, “An artificial intelligence system for detecting the types of the epidemic from X-rays: Artificial intelligence system for detecting the types of the epidemic from x-rays,” in *2022 27th International Computer Conference, Computer Society of Iran (CSICC) Iran*, Tehran-Iran, pp. 1–6, 2022. https://doi.org/10.1109/CSICC55295.2022.9780523

[37] P. Sharma, R. Arya, R. Verma and B. Verma, “Conv-CapsNet: Capsule based network for COVID-19 detection through X-Ray scans,” *Multimedia Tools And Applications*, pp. 1–25, 2023. https://doi.org/10.1007/s11042-023-14353-w

[38] S. Qiu, “IRCM-Caps: An X-ray image detection method for COVID-19,” *The Clinical Respiratory Journal*, pp. 1–10, 2023. https://doi.org/10.1111/crj.13599

[39] L. Zhao, X. Wang and L. Huang, “An efficient agreement mechanism in CapsNets By pairwise product,” *arXiv Preprint*. arXiv:2004.00272, 2020.

[40] “Understanding capsule network architecture,” *Intel*, https://www.intel.com/content/www/us/en/developer/articles/technical/understanding-capsule-network-architecture.html

[41] S. Kurumalla and P. S. Rao, “K-nearest neighbor based DBSCAN clustering algorithm for image segmentation,” *Journal of Theoretical and Applied Information Technology*, vol. 92, no. 2, pp. 395, 2016.

[42] A. Abid, A. Abdalla, A. Abid, D. Khan, A. Alfozan *et al.,* “Gradio: Hassle-free sharing and testing of ML models in the wild,” accessed Feb. 10, 2022, 2019. [Online]. Available: https://arxiv.org/abs/1906.02569v1

[43] A. Abid, A. Abdalla, A. Abid, D. Khan, A. Alfozan *et al.,* “An online platform for interactive feedback in biomedical machine learning,” *Nature Machine Intelligence*, vol. 2, no. 2, pp. 86–88, 2020.